CORRELATIONS FOR SOOT AND SMOKE-POINT IN MOMENTUM CONTROLLED LUMINOUS LAMINAR JET DIFFUSION FLAMES (in space)

By

Michael A. Delichatsios
Senior Manager / Technical Director
FIRE SCIENCE AND TECHNOLOGY LABORATORY / CSIRO
PO Box 310, North Ryde NSW 1670
AUSTRALIA

Email: michael.delichatsios@dbce.csiro.au

ABSTRACT

Simple correlations for flame envelop and soot production are developed for non-buoyant
laminar jet flames in microgravity (space). First, the characteristics of the flow field and flame
envelop(height and width) are expressed in terms of input parameters both for high momentum(parabolic flow) and low momentum (elliptic flow) jet flames. Soot formation rate relations are extended from previous work on buoyant laminar smoke-point flames and used for the present non-buoyant jet flames. Together with the flow characteristics, they provide predictions of soot concentration and smoke-point flame development in microgravity. These predictions are substantiated and verified by using recent experiments in space for flame shapes and soot in non-buoyant luminous Hydrocarbon / Air jet flames.

INTRODUCTION

In a recent review [1], a detailed background discussion of laminar jet diffusion flames is presented. Emphasis is given to the difference of flow fields between buoyant (ground) and momentum controlled (space) laminar jet flames in reference to soot formation and smoke yields. New experimental data on purely momentum controlled jet flames in space are presented in [1] as well in a more recent publication [2]. The analysis used in [1,2] for the flame envelope (flame height and visible flame shape) has been presented in previous publications by the same group[3,4]. It is based on a laminar jet flame analysis by Spalding [5].

We present a different analysis of momentum dominated (non-buoyant) laminar jet flames in this work. One difference from previous analysis in [1,2,3,4] in distinguishing two regimes for these jet flames, high momentum and low momentum regimes. The application and analysis in [1,2] is limited to the first regime. We compare the present analysis with the experimental results in [1,2,3,4]. We suggest that there is no need to use virtual origin as is done in [1,2] to fit the experimental results for flame height.

But the main contribution of this paper is to use these simple correlations for the flow together with a global soot formation model [6] to provide an interpretation of the data for soot concentrations in non - buoyant flames [1,2].

First we review the soot formation model, followed by a presentation of dimensional analysis of non-buoyant jet diffusion flames. These results are then combined to develop predictions and validations for soot concentrations and smoke-point flames in jet flames in microgravity.

REVIEW OF SOOT FORMATION MODEL FROM RESULTS IN BUOYANT JET FLAMES

Laminar diffusion flames buoyant or non-buoyant possess similarity [1,2,3,4,6,7] so that soot formation kinetics and soot concentrations can be expressed in terms of simple characteristic quantities.

The concept and measurements of smoke-point laminar diffusion flames [6 where also other previous references are cited] have been the basis for developing the following soot chemistry related quantities:

- Soot formation time
- Maximum soot concentration inside the flame envelope
- Conditions (e.g. flow rate) at which smoke emerges from flame tip.

From the comprehensive development of smoke point flames [6], we have extracted results that are pertinent in analysing the experimental smoke-point flames in non-buoyant laminar jet flames in microgravity in [1,2,3.4].

These results are:

1. The characteristic soot formation time, C_s, which depends on the fuel chemistry and the structure of the laminar flow. For the same type of laminar flow (laminar diffusion flame, buoyant or momentum, counterblow) and the same fuel this time is inversely proportional to density (pressure) [6]:

$$\tau_s \propto p^{-1} \qquad (1)$$

2. The maximum soot mass concentration is proportional to a characteristic flow time divided by the soot formation time [6]:

$$Y_s = \frac{\tau_F}{\tau_s} \qquad (2)$$

3. The smoke point height is determined by the requirement that the radiant fraction at these conditions takes a fixed value causing extinction of the flames near the tip of the flame. This radiant fraction for optically thin flames is :

$$\chi_{r,s} = \frac{\sigma T_f{}^4 V_f \phi_s}{\dot{Q}} = c \qquad (3)$$

Here V_f is the flame volume, T_f is a flame temperature for radiation losses and ϕ_s is the soot volume fraction. This is related to the soot mass fraction as:

$$\phi_s = \frac{\rho_g}{\rho_s} Y_s \qquad (4)$$

where ρ_g and ρ_s are gas and soot densities.

In order to apply these relations in Equ.(1,2,3,4) , residence flow times and the flame volume for laminar diffusion flames in microgravity are obtained in the next section. Similar relations have been developed for buoyant flames [5,6] and non-buoyant flames [1,2,3,4,5].

DIMENSIONAL ANALYSIS OF THE RESULTS TO NON-BUOYANT LAMINAR JET FLAMES

The characteristic scales for are the flow time, the velocity at the flame tip, the flame width and the flame height.

The flow time is given by:

$$\tau_F = \frac{L_f}{u_f} \qquad (5a)$$

where L_f is the flame length and u_f is the velocity at the flame tip. The flame height is determined as the axial location wherein the centerline mixture fraction is stoichiometric.

These quantities, namely flame height and velocity at flame tip, can be determined in the following way:

1)Mass flow at the flame tip satisfies the following relation:

$$\rho_f u_f \delta_f^2 = \dot{m}_s (S+1) \qquad (5b)$$

Here ρ_f is the flame density , δ_f the jet width at the flame tip, $\dot{m}_s$ the supply flow rate at the source and S the air to fuel mass stoichiometric ratio.

2)Relation of diffusion time to residence time is given by the following equation:

$$\frac{L_f}{u_f} = \frac{\delta_f^2}{\nu_f} \qquad (5c) \quad \text{where } \nu_f \text{ is the kinematic viscosity at the flame temperature.}$$

Iin contrast to [1,2], we do not consider the Schmidt number effects in the present approach. The effects of non-unity Schmidt numbers depend on the velocity profile where molecular diffusion occurs. For the non-buoyant laminar jet flames, the non-unity Schmidt effects are weak for the range of .5 to 2 as one can see using the exact solution that assumes constant properties [8].

3) For the momentum balance there are two possibilities:

3a) <u>If momentum is large</u>, an additional equation to be used (together with 5b and 5c) is the momentum conservation equation:

$$\rho_f u_f{}^2 \delta_f{}^2 = \dot{M}_S = \text{momentum at source} \quad (6)$$

This conservation relation expresses the boundary layer (parabolic) like behavior of the jet flow at high momentum values. It also forms the basis for the analysis in [1,2,3,4 or 5].

3b) If momentum is small, the previous equation is replaced by:

$$L_f = \delta_f = \frac{\nu_f}{u_f} \quad (7)$$

In this case, momentum is conserved again but one must account for pressure variations because the flow field is elliptic near the source.
For these two separate situations, we obtain the following characteristic values for the jet properties:

LARGE JET MOMENTUM (use Equations 5b, 5c, and 6)

$$L_f = \frac{\dot{m}_s(S+1)}{\mu_f} \quad (8a)$$

$$u_f = \frac{\dot{M}_S}{\dot{m}_s(S+1)} = \frac{u_s}{S+1} \quad (8b)$$

$$\delta_f = \sqrt{\nu_f \frac{L_f}{u_f}} \quad (8c)$$

which reduces to

$$\frac{\delta_f}{d_s(S+1)} = cons\tan t \quad (8d)$$

wherein Equation 8a and 8b have been used. Moreover, d_s is the nozzle diameter.
SMALL JET MOMENTUM (use Equations 5a, 5b, 7)

$$L_f \propto \delta_f = \frac{\dot{m}_s(S+1)}{\mu_f} \quad (9a)$$

$$u_f = \frac{\mu_f \nu_f}{\dot{m}_s(S+1)} \quad (9b)$$

The relations in equations 8 and 9 are used to determine predictions of soot concentration and smoke-point flame conditions for the experiments of laminar jet diffusion flames in space [1,2]. Because of lack of buoyancy, these are momentum-controlled flames that were conducted at variable pressures. One should notice that the flame height in both cases 8a and 9a is given by the same expression but the proportionality coefficients may be different. We do not have enough data to support this differentiation. It is possible, however, to plot existing data in the following way:

$$L_f / (\frac{\dot{m}_s(S+1)}{\mu_f}) \text{ versus Re at the source } Re_s = \frac{u_s d_s}{\nu_s} = \frac{4}{\pi} \cdot \frac{\dot{m}_s}{\mu_s d_s} \quad (9c)$$

(Schmidt number effects are neglected, see discussion following Equ.5c. An additional length ratio d_s/L_f is needed to complete the set of dimensionless variables. For the same stoichiometric ratio ,S , this length scale ratio is the same as in Equ. 9c)

We present a plot of some data [1,2,7] in Figure 1. Figure 7 of [7] points out that for small Reynolds numbers and the same fuel, the flame height ratio in equation 9c is larger than for large Reynolds numbers. This is also clear for Methane, Ethane and Propane microgravity drop tower data in ref. 3 as shown in Figure 2a and 2b reproduced here from [3]. At High Reynolds numbers, the data from that paper (dark symbols) indicate that flame height ratio decreases with Re Number. Transition from low to high momentum regime seems to occur at a source Re number of 100.
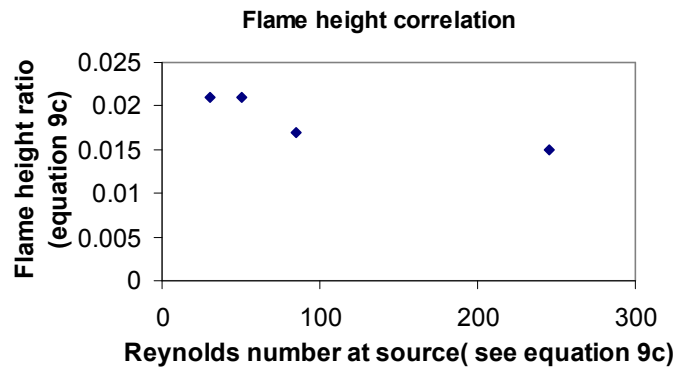

Figure 1. Flame height correlation for non-buoyant laminar diffusion flames. Data for two lower Reynolds number from [1,2] and for the other from [7].

Figure 2b   Qualitative illustration of flame lengths for non-buoyant flames included in Figure 2a.
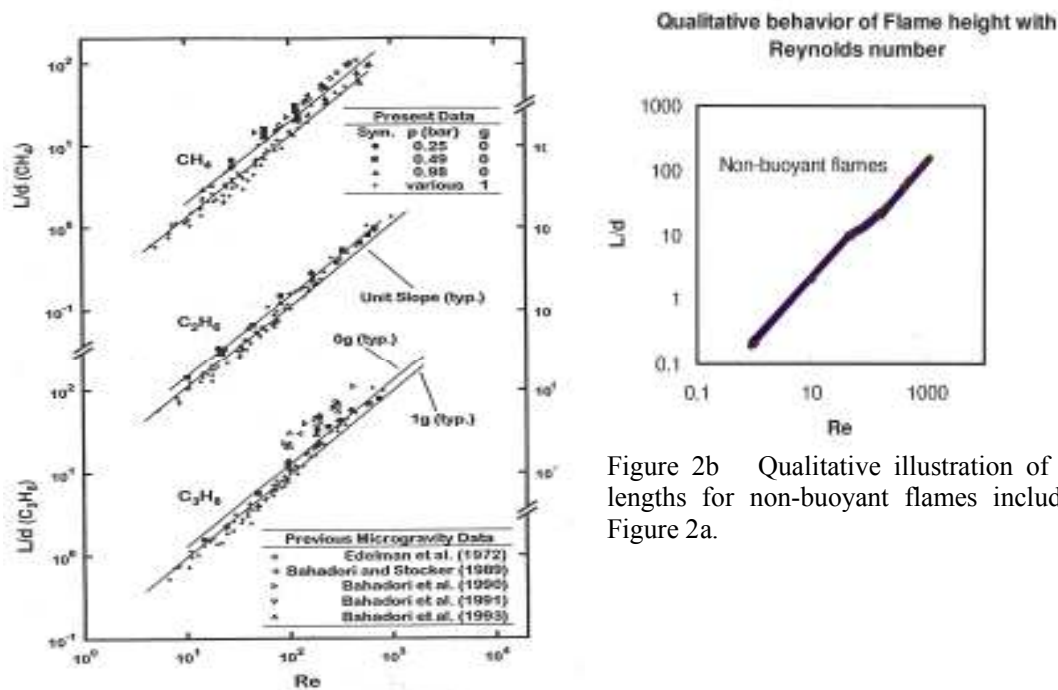
Figure 2a. Stoichiometric (flame) lengths of buoyant and non-buoyant flames taken from reference 3. Present data refers to data in reference 3. Previous data refers to data as described in reference 3.

The flame width can be expressed in general (using equations 8c and 9a) as :

$$\frac{\delta_f}{d_s(S+1)} = function(\frac{u_s d_s}{v_s}) \quad (9d)$$ Here the subscript s denotes properties at the source.

For the **high jet momentum case**, the Left Hand Side of Equation 9d is constant as in Eq. 8d. In contrast, for the **low jet momentum case** the LHS of Eq. 9d should be proportional to its RHS , namely:

$$\frac{\delta_f}{d_s(S+1)} \propto \frac{u_s d_s}{v_s} \quad (9e)$$

This relation is also derived from Equation 9a. Contrary to the authors' claims [4], the results for the flame width as plotted in Fig 5 of reference 4 support a relation similar to Equ. 9e than a relation as given by Equation 8d, according to the claim in [4].

This difference in flame width behavior has also been noted in ref. 3 from which the following statement is extracted.: " Non- buoyant widths exhibit different behavior in the low- and high-Re regimes. At low Re, nonbuoyant flames tend towards sphericity and thus $\frac{\delta_f}{d_s}$ increases with Re similar to the behavior of flame lengths. However, for source Reynolds numbers exceeding 100, flames become elongated and normalized widths remain fixed regardless of Re."

SOOT CONCENTRATION PREDICTIONS
Two cases are considered again:

LARGE JET MOMENTUM- soot concentration (equations 8)
We use equation 2, 5a and equations 8 to find out a characteristic soot concentration:

$$Y_s = \frac{\{\dot{m}_s(S+1)\}^2}{\mu_f \dot{M}_s} \frac{1}{\tau_s} \quad (10a)$$ or in terms of the source diameter and density

$$Y_s = \frac{(S+1)^2 d_s^2}{\mu_f} \frac{\rho_{gs}}{\tau_s} \quad (10b)$$

For varying pressures this relation becomes:

$$Y_s = \frac{(S+1)^2 d_s^2}{\mu_f} \frac{\rho_{gso}}{\tau_{so}}(\frac{p}{p_o})^2 \quad (10c)$$ where equation 1 has been also used. The subscript "so"

denotes property values at a reference pressure p_o. Notice that the flame height (8a) or the flame width (8c) are independent of pressure.

The soot volume fraction behaves with pressure as (using also Equation 4) :

$$\phi_s = \frac{\rho_g}{\rho_{soot}} Y_s = \frac{(S+1)^2 d_s^2}{\mu_f} \frac{\rho_{gs}}{\tau_s} \frac{\rho_g}{\rho_s}$$ or in terms of pressure variation:

$$\phi_s = \frac{(S+1)^2 d_s^2}{\mu_f} \frac{\rho_{gs}}{\tau_s} \frac{\rho_g}{\rho_s} \propto \frac{(S+1)^2 d_s^2}{\mu_f} \frac{\rho^2_{gso}}{\tau_{so}}(\frac{p}{p_o})^3 \quad (10d)$$

These relations show that a characteristic soot concentration is independent of flow rate and changes as the third power of pressure. To verify this relation we use the limited results in ref. 2.

The characteristic soot concentration is the maximum for the flames reported in Figures 1, 5 and 6 of [2] at pressures 65 , 100 and 50 kPa. for the same nozzle diameter 1.6 mm. The maximum soot concentration is taken for flames at 50, 65 and 100 kPa before the smoke escapes from the top of the

flames as 2, 4 and 20 ppm respectively. One should also notice that the flow rate for the 65 kPa flame is .91 mg / s whereas it is 1.84 mg / s for the other two flames. These flames are beyond the smoke point conditions (at 50 and 100kPa) or near smoke –point conditions (at 65kPa) for the respective pressures as shown in Figure 4 of [2]. It is expected that they can be described by the present case wherein the momentum dominates the flow properties.   Figure 3 demonstrates this relationship. It seems that these flows correspond to the high momentum regime because the Reynolds number is 141 for the 50kPa and 100kPa flames and 70 for the 65kPa flame.
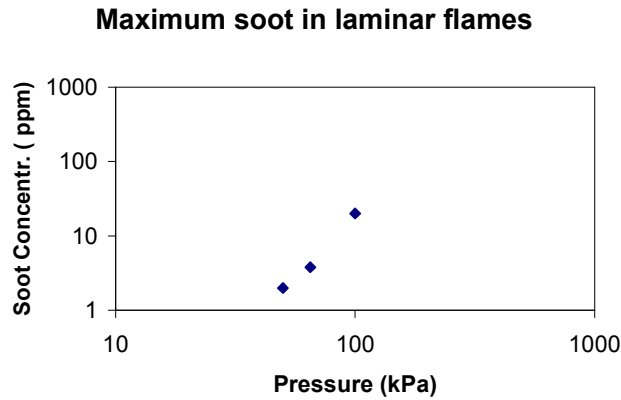
Maximum soot in laminar flames

Figure 3. Maximum soot concentrations in three nonbuoyant flames at 50,65 and 100kPa for a nozzle diameter 1.6mm and flow rates of ethylene 1.84, .91 and 1.84 mg /s respectively [1,2].

SMALL JET MOMENTUM -soot concentration (use equation 9)
The characteristic soot mass concentration is obtained from equation 2, 5a and 9 :

$$Y_s = \frac{\{\dot{m}_s(S+1)\}^2}{\mu_f^2 \nu_f} \frac{1}{\tau_s} \qquad (11a)$$

For varying pressure this equation becomes:

$$Y_s = \frac{\{\dot{m}_s(S+1)\}^2}{\mu_f^3} \frac{\rho_{fo}}{\tau_{so}} (\frac{p}{p_o})^2 \qquad (11b)$$

The soot volume fraction is :

$$\phi_s = \frac{\{\dot{m}_s(S+1)\}^2}{\mu_f^3} \frac{\rho_{fo}}{\tau_{so}} \frac{\rho_{go}}{\rho_s} (\frac{p}{p_o})^3 \quad (11c)$$

Equations 10d and 11c show that the maximum soot concentration has the same dependence on pressure but different dependence on fuel flow rate for the high and low momentum regime. For the high momentum case (Equ. 10d) the characteristic soot volume fraction is independent of the flow rate as also illustrated in Figure 3.

SMOKE- POINT FLAMES

As we pointed out, Eq. 3 determines the condition for a smoke-point flame. As we did before we consider two cases:
 LARGE JET MOMENTUM – smoke-point (use equations 8)
To use Equation 3, we need the flame volume . This volume is for the present case :

$$V_f = L_f \delta_f^2 = \nu_f \frac{L_f^2}{u_f} = \nu_f \frac{(\dot{m}_s(S+1))^3}{\mu_f^2 \dot{M}_s} \quad (12a) \text{ wherein equations 8 have been used.}$$

By inserting equation 12a and equation 10d into equation 3 , one obtains:

$$\chi_{r,s}/\sigma T_f^{\,4} = \frac{(S+1)^5}{\mu_f^{\,2}\Delta H_c}\,d_s^{\,4}\,\frac{\rho_{gso}^{\,2}}{\tau_{so}}\Big(\frac{p}{p_o}\Big)^3 \qquad (12b)$$

where the relation $\dot{Q} = \dot{m}_s \Delta H_c$ has been also used.

For a smoke-point flame to be developed, the radiant fraction has to be greater than a critical value about 0.3 [6]. Assuming that the flame temperature does not vary much with pressure, smoke-point conditions will occur when the value of equation 12b becomes greater than a fixed value. For the present high momentum regime, it is obvious from equation 12b that smoke emission will occur only for source diameter greater than a certain value. For small source diameters, no smoke emission will occur. These conditions are independent of the mass supply rate as equation 12 b shows.

This result has been implicitly verified by experiments using small nozzles, namely .195mm in diameter, where no smoke escapes for any high flow rate [7] and using larger nozzles in space, 1.6 mm or larger where smoke always escapes for high flow rates[1,2,3,4].

For the same nozzle however, as the fuel flow rate decreases Equ. 8 ceases to be applicable and Equation 9 is relevant for smoke-flame conditions , as examined next.

SMALL JET MOMENTUM – smoke point(use equation 9)
Equation 3 for the radiant fraction becomes:

$$\chi_{r,s}/\sigma T_f^{\,4} = \frac{V_f \phi_s}{\dot{Q}} = \frac{\delta_f^{\,3}\phi_s}{\dot{Q}} =$$

$$= \frac{(\dot{m}_s(S+1))^3}{\mu_f^{\,3}\dot{m}_s\Delta H_c}\,\frac{(\dot{m}_s(S+1))^2}{\mu_f^{\,3}}\,\frac{\rho_{fo}}{\tau_{so}}\,\frac{\rho_{go}}{\rho_s}\Big(\frac{p}{p_o}\Big)^3 = \qquad (13a)$$

$$= \frac{(S+1)^5}{\mu_f^{\,6}\Delta H_c}\,\frac{\rho_{fo}}{\tau_{so}}\,\frac{\rho_{go}}{\rho_s}\,\frac{\dot{m}_s^{\,4}\,p^3}{p_o^{\,3}}$$

where equations 9 have been used. Smoke points will occur when this value of this expression is greater than a critical value. This condition is now independent of the nozzle diameter and is determined by:

$$\dot{m}_s \propto p^{-3/4} \qquad (13b)$$

This is consistent with the results of Figure 4 taken from [2] where the smoke point height (proportional to heat release rate and mass flow rate) in the space experiments is shown to a) vary a little less than inversely proportional to pressure and b) be independent of nozzle diameter. For comparison and contrast the smoke-point height (or heat release rate) decreases inversely proportional to pressure [6].
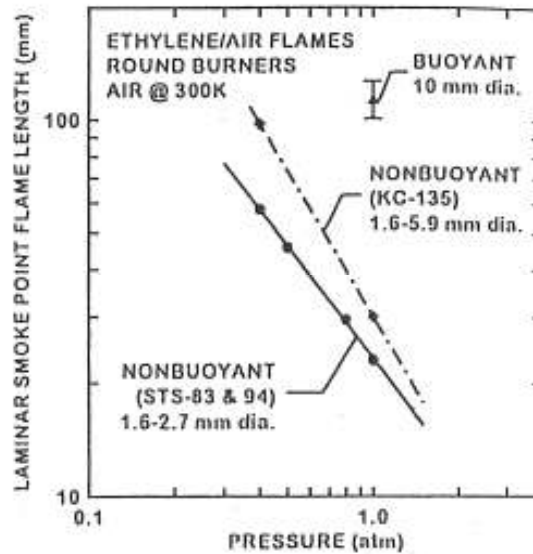
Figure 4. Laminar smoke-point flames taken form [2]. The decrease of smoke-point lengths with pressure is somewhat less than inversely proportional to pressure for the space experiments. They are also independent of nozzle diameter in consistency with Equation 13a and 13b.

SOME GENERAL COMMENTS

The major results from this work are:

1. The same flow and soot similarity parameters as in buoyant laminar jet flames can be used for non-buoyant jet flames as shown in equations 1,2,3 and 4.
2. Two flow cases are considered for non-buoyant laminar jet flames a) dominated by the source momentum (see equations 8a,8b, 8c) and b) dominated by the viscosity (equations 9a and 9b). in both cases, the flame height is given by the same expression but the proportionality constant may be different, see Figure 1 (see equation 8a nd 9a). However, the characteristic flow time is different in these cases.
3. The analysis of the conditions for a smoke point to be developed shows that there is a source diameter that delineates two regimes: a) for diameters smaller than this diameter and high momentum flows, no smoke escapes from the flames(see ref. 7 where d_s = .195 mm) and b) for larger diameters and high momentum flows smoke always escapes from the flames [1,2]. This conclusion follows the derivation of equation 12b.
4. The same analysis for the smoke point flames shows that as the mass flow rate decreases the flow is dominated by viscosity (not source momentum). This occurs not only because the momentum at the source is small but also because the viscosity increases due to high flame temperatures (see equation 9a and 9b). As a consequence a critical fuel mass flow rate exists at which a smoke point flame develops. This flow rate is independent of nozzle diameter (see equation 13 a and 13 b) and decreases with pressure as the ¾ power of pressure see also figure 4.
5. The present analysis also predicts the variation of maximum soot concentration with pressure as shown in Figure 3 for the case of non-buoyant laminar (momentum) dominated flames.

REFERENCES

1. Urban D.L., Yuan Z.-G., Sunderland P.B, Linteris G.T., Voss J.E., Lin K.-C., Dai Z.,Sun K., Faeth G.M. " Structure and soot properties of nonbuyoant ethylene/ air laminar jet diffusion flames" AIAA Journal, 36. 8 ,1998.
2. Lin K.-C., Z.Dai and G.M.Faeth " Laminar Soot Processes" pg 133 , Fifth International Microgravity Combustion Workshop , NASA , May 1999.
3. Sunderland,P.B., Mendelson B.J., Yuan Z.-G., Urban D.L. " Shapes of Buoyant and Nonbuoyant Laminar Jet Diffusion Flames " *Combust.Flame* 116,376-386, 1999
4. Lin K.-C, Faeth G.M, Sunderland P.B,Urban D.L., Yuan Z.-G., "Shapes of Nonbuoyant Round Luminous Hydrocarbon?Air Laminar Jet Diffusion Flames" *Combust. Flame* 116, 415-431 , 1999.
5. Spalding, D.B., *Combustion and Mass Transfer* Pergamon, New York,1979, p185.
6. Delichatsios, M.A. , " A Phenomenological Model for Smoke-Point and Soot Formation in Laminar Flames " Combust. Science and Tech., 100, pp 283-298, 1994.
7. Chung, S.H. and B.J.Lee "On the Characteristics of Laminar Lifted Flames in a Nonpremixed Jet" Combustion and Flame , 86,62-72,1991.
8. Kuo, K.K., *Principles of Combustion,* Wiley , New york,1986, pp.360-365.

Nomenclature

English

d_s nozzle diameter

L_f flame height

$\dot{m}_s$ mass flow rate at the nozzle

$\dot{M}_s$ momentum flux at the source

p , p_o pressure, reference pressure

$\dot{Q}$ heat release rate

$\dot{Q}_s$ heat release rate at smoke-point

T_f characteristic flame radiation temperature

u_f u_s velocity at flame tip, velocity at source

V_f flame envelop volume

Y_s soot mass fraction

Greek

ΔH_c heat of combustion per fuel mass

δ_f maximum flame width

μ_f dynamic viscosity at flame temperature

ν_f kinematic viscosity at flame temperature

ρ_g gas density

ρ_s soot density

ρ_f gas density at flame temperature

ρ_{gs} gas density at source

ρ_{gso} gas density at source at reference pressure p_o

C   Boltzmann constant

τ_F flow time (Equ. 5a)

τ_S , τ_{SO} soot formation time, soot formation time at reference pressure p_o

$\chi_{r,S}$ radiation loss fraction at smoke-point conditions

FIGURE TITLES

Figure 1. Flame height correlation for non-buoyant laminar diffusion flames. Data for two lower Reynolds number from [1,2] and for the other from [7].

Figure 2a. Stoichiometric (flame) lengths of buoyant and non-buoyant flames taken from reference 3. Present data refers to data in reference 3. Previous data refers to data as described in reference 3.

Figure 2b   Qualitative illustration of flame lengths for non-buoyant flames included in Figure 2a.

Figure 3. Maximum soot concentrations in three nonbuoyant flames at 50,65 and 100kPa for a nozzle diameter 1.6mm and flow rates of ethylene 1.84, .91 and 1.84 mg /s respectively [1,2].

Figure 4. Laminar smoke-point flames taken form [2]. The decrease of smoke-point lengths with pressure is somewhat less than inversely proportional to pressure for the space experiments. They are also independent of nozzle diameter in consistency with Equation 13a and 13b.